



PCCP

**In Silico Mutational Analyses Reveal Different Ligand-Binding Abilities of Double Pockets of Medaka Fish Taste Receptor Type 1 Essential for Efficient Taste Recognitions**

Journal:	<i>Physical Chemistry Chemical Physics</i>
Manuscript ID	CP-ART-06-2021-002876.R1
Article Type:	Paper
Date Submitted by the Author:	11-Aug-2021
Complete List of Authors:	Aida, Hayato; University of Tsukuba Morita, Rikuri; University of Tsukuba, Center for Computational Sciences Shigeta, Yasuteru; University of Tsukuba, Physics Harada, Ryuhei; Tsukuba University, Center for Computational Sciences

SCHOLARONE™  
Manuscripts

***In Silico* Mutational Analyses Reveal Different Ligand-Binding Abilities of  
Double Pockets of Medaka Fish Taste Receptor Type 1  
Essential for Efficient Taste Recognitions**

Hayato Aida<sup>1†</sup>, Rikuri Morita<sup>2†</sup>, Yasuteru Shigeta<sup>1,2</sup>, and Ryuhei Harada<sup>1,2\*</sup>

<sup>†</sup> Equally Contributed

\*E-mail: ryuhei@ccs.tsukuba.ac.jp

<sup>1</sup>Master's Program in Biology, University of Tsukuba, 1-1-1 Tennodai, Tsukuba, Ibaraki 305-8577 Japan

<sup>2</sup>Center for Computational Sciences, University of Tsukuba, 1-1-1 Tennodai, Tsukuba, Ibaraki 305-8577

Japan

**Abstract**

Taste receptors are important sensors for the detection of nutrient concentrations in animals. Tastes are recognized by interactions between chemical substances and taste receptors. Recently, the high-resolution X-ray crystal structure of the extracellular ligand-binding domains (LBDs) of medaka fish (*Oryzias latipes*) taste receptor type 1 (T1r) complexed with the ligands (amino acids) was determined. The medaka fish T1r is a heterodimer composing of two different LBDs, T1r2aLBD and T1r3LBD. In this study, we performed all-atom molecular dynamics (MD) simulations on this heterodimer (T1r2aLBD – T1r3LBD) to address mutational effects on key residues nearby each ligand-binding pocket in recognizing one of the ligands (L-

Gln). For T1r2aLBD, Ser165 was important in ligand recognition owing to its direct hydrogen bond with the ligand. After mutating Ser165 to Ile or Ala, the direct hydrogen bonds between the ligand and the binding pocket were weakened, which destabilized the ligand-binding form of T1r2aLBD. For T1r3LBD, Ser300 was important in the ligand recognition. The water-mediated hydrogen bond with the side-chain hydroxyl group of Ser300 is a single interaction to maintain the ligand-binding form of T1r3LBD. After mutating Ser300 to Glu or Ala, both mutant systems almost maintained their ligand-binding form. As a mechanism for maintaining the binding form of T1r3LBD, alternative hydrogen bonds were formed as direct interactions instead of the indirect water-mediated interactions found in the wild-type system, which stabilized the binding form of T1r3LBD. Judging from our *in silico* mutational analyses, T1r2aLBD was structurally destabilized by the amino acid mutations. Therefore, it might be required that the ligand-binding pocket of T1r2aLBD is composed of a set of specific residues to maintain its ligand-binding form. On the contrary, T1r3LBD was robust to withstand the amino acid mutations. These different ligand-binding abilities of both LBDs provide multiple binding modes, which might be helpful for discriminating various taste substances or detecting concentrations of nutrients efficiently.

## 1. Introduction

Taste receptors are important sensors for the detection of nutrient concentrations in animals. Tastes are recognized as responses induced by specific interactions between chemical substances and taste receptors.<sup>1</sup>

<sup>2</sup> Animals have a taste receptor type 1 (T1r) family that recognizes a variety of sweetness or umami (savory tastes) included in the nutrients such as sugars and L-amino acids.<sup>3-5</sup> Structurally, the T1r family is categorized into the class C G-protein-coupled-receptor (GPCR) family.<sup>6</sup> This family is conserved vertebrates, including

fishes, birds, and mammals.<sup>7</sup> These kinds of receptors function as constitutive heterodimers such as T1r1–T1r3 and T1r2–T1r3.<sup>3, 5</sup> Depending on each heterodimer, ligand specificity is adjusted to each diet of each animal.<sup>3-5, 8</sup> Taste substances are mainly recognized by extracellular ligand-binding domains (LBDs) of T1r proteins. In previous studies, mutation and modelling/docking studies have revealed that LBDs of T1r heterodimers recognize major sweet and umami taste substances.<sup>9-15</sup>

As an example of T1r, a structural model of the medaka fish (*Oryzias latipes*) T1r consists of the extracellular LBDs, Cys-rich domains, and a transmembrane membrane (TM) domain. The Cys-rich domains function as linkers to connect LBDs and the TM domain. Each LBD consists of approximately 500 amino acid residues and is divided into two subdomains (LB1 and LB2). The taste substances are recognized by the ligand-binding to each LBD. Each taste substance binds to each cleft of LB1 and LB2. Upon ligand-binding to these extracellular LBDs, the receptor is activated, leading to signal transduction to the heterotrimeric G-protein in the cytoplasm. Thus, each LBD plays an essential role in recognizing the taste substance. In previous studies, a mechanism of signal transduction of T1r has been reported using other class C GPCR LBDs.<sup>16, 17</sup> More specifically, in both LBDs, the open-to-closed transitions between LB1 and LB2 are induced upon ligand-binding to these clefts, accompanied by configurational rearrangements.<sup>18</sup> A series of these structural transitions propagated to the downstream transmembrane domain activates the heterotrimeric G-protein.

It has been difficult to determine the T1r structure owing to its heterologous expression. However, advances in experimental techniques enabled the recent high resolution determination of the X-ray crystal structure of the heterodimer of the extracellular LBDs of the medaka fish T1r complexed with ligands (amino acids).<sup>19</sup> The heterodimer revealed by the X-ray crystallography consists of T1r2-subtype LBD (T1r2aLBD)

and T1r3LBD (Fig. 1(a)). Both LBDs individually recognize taste substances (ligands, such as amino acids). This X-ray crystallography study evaluated the ligand-binding ability of both LBDs by calculating the  $\Delta G$  values from their crystal structures. In addition, the structural study evaluated the differences in the estimated  $\Delta G$  values ( $\Delta\Delta G$ ) between the various amino acid binding and L-Glutamine (L-Gln) binding to both LBDs. The  $\Delta\Delta G$  values correlated with those derived from experimental binding assays for T1r2aLBD-T1r3LBD by fluorescence resonance energy transfer. The experimentally estimated  $\Delta\Delta G$  values indicate that T1r2aLBD and T1r3LBD preferentially recognize L-Gln over other amino acids such as L-Ala, L-Arg, L-Glu, and Gly. In this study, we focused on L-Gln that shows the highest binding ability for T1r2aLBD-T1r3LBD as a ligand. Figures 1(b-c) show how L-Gln is arranged near the binding pocket of T1r2aLBD and T1r3LBD in the X-ray crystal structure. For T1r2aLBD, its binding pocket recognizes L-Gln with multiple hydrogen bonds. T1r2aLBD maintains its binding form using two types of interactions with L-Gln. The surrounding residues near the binding pocket interact with L-Gln directly or indirectly. As a direct interaction, the  $\alpha$ -amino and carboxyl groups of L-Gln form hydrogen bonds with these key residues near the binding pocket. These groups of L-Gln interact with the main-chain amide and side-chain hydroxyl groups of Ser142 and Ser165 of T1r2aLBD. On the contrary, as an indirect interaction, the water-mediated hydrogen bonds are dominant through the side-chain carboxyl group of Asp288 and Asp289 of T1r2aLBD, as previously reported.<sup>19</sup>

In addition to the structural analysis of the medaka fish T1r, several point mutations were considered for the human T1r to address the ligand-binding responses of both LBDs.<sup>19</sup> The human T1r forms a heterodimer consisting of T1r2LBD and T1r3LBD with different amino acid sequences from the medaka fish T1r. Mutagenesis analyses indicated that point mutations on T1r2LBD at the binding pocket (S165I and

S165A) cause a loss of or a weakened response to the L-amino acids. In contrast, a point mutation on T1r3LBD at the binding pocket (S300E) maintains the structural stability of the ligand-binding form. These essential residues near the binding pocket of LBDs are well-conserved in amino acid sensing taste receptors of T1r1 and most classes of C GPCRs.<sup>6</sup>

Based on these mutagenesis analyses of the human T1r, this study computationally addressed how these point mutations affect the responses involving the recognition of the ligands of both LBDs in medaka fish. As previously described, the key residues near the binding pockets have been conserved in several species. Therefore, we considered the same point mutations for medaka fish. From a computational point of view, to address these mutational effects, we performed all-atom molecular dynamics (MD) simulations for the wild-type (WT) and mutants of the extracellular LBDs of the medaka fish T1r (Table 1). The all-atom MD simulations enable one to analyze possible perturbations from the point mutations in the atomic level, which might be a novelty of this study since we can follow detailed interactions between each ligand and each residue nearby each binding pocket. As dynamical and structural analyses for these mutational effects, we also calculated the ligand-binding abilities of LBDs. More specifically, by evaluating the ligand-binding abilities of both LBDs, we clarify how their different ligand-binding abilities are helpful for discriminating taste substances in the medaka fish T1r, which might be a new insight for the taste recognition mechanism of this heterodimer (T1r2aLBD–T1r3LBD).

## **2. Materials and Methods**

### **2.1 Setup of MD Simulations on the Extracellular LBDs of the Medaka Fish T1r**

As an initial configuration, an all-atom system of the heterodimer (extracellular LBDs) of the medaka fish T1r was modeled using the X-ray crystal structure (PDBid: 5X2M, Fig. 1).<sup>19</sup> The X-ray crystal structure was solvated with the TIP3P water model<sup>20</sup> and neutralized with counter ions in a rectangular box using the GROMACS tool.<sup>21</sup> For the ligand, L-Gln was chosen to form the complex. From the experimental measurement in the previous study, L-Gln shows the highest binding ability over other amino acids.<sup>19</sup> The crystal structure indicates that L-Gln interacts with the binding pocket of T1r2aLBD via the characteristic interactions (the direct/indirect interactions shown in Figs. 1(b-c)). Judging from the highest ligand-binding ability and these specific interactions, L-Gln was chosen as a representative taste substance to form the complex. To increase the time step of MD, the chemical bonds of the solute and the water molecules were treated with the LINCS and SETTLE algorithms,<sup>22,23</sup> respectively. The system temperature and pressure were controlled using the modified Berendsen thermostat<sup>24</sup> and the Parrinello–Rahman method,<sup>25, 26</sup> respectively. The electrostatic interactions were evaluated with the particle mesh Ewald method<sup>27</sup> using a real-space cutoff of 10.0 Å. The cutoff value for van der Waals interactions was set to 10.0 Å. All-atom MD simulations were performed with the GPU version of GROMACS 2019 package<sup>21</sup> using the AMBER ff03 force field.<sup>28</sup> To establish a parameter of L-Gln, its restrained electrostatic potential (RESP) charges were calculated based on the gas-phase HF/6-31(d) quantum mechanics calculations. Based on the RESP charges, the AMBER tool (antchamber)<sup>29</sup> generated a set of parameters for L-Gln. The initial configuration was energetically minimized before starting the MD simulations. After minimization, a 100-ps MD simulation was performed under *NVT* ( $T = 300$  K). Subsequently, a 100-ps MD simulation was performed under *NPT* ( $T = 300$  K and  $P = 1$  bar). Finally, the relaxed snapshot was regarded as the starting configuration of the production run, which was run

on the WT system.

## 2.2 Evaluations of Ligand-Binding Free Energies on the WT and Mutant Systems

For ligand recognition, a prior mutagenesis analysis of the human T1r reported the key residues of LBDs.<sup>19</sup> Based on the previous study, we considered the mutational effects on the corresponding amino acids in the medaka fish T1r using the all-atom MD simulations. Table 1 shows the WT and its mutants of the extracellular LBDs of the medaka fish T1r. Each mutant was modeled in terms of the relaxed heterodimer of the WT system by replacing the corresponding residues. For each system, five 200-ns MD runs were independently performed under *NPT* ( $T = 300$  K and  $P = 1$  bar) by changing their initial velocities to obtain statistically reliable trajectories. To quantitatively evaluate the ligand-binding free energies of the WT and the mutant system, we adopted the molecular mechanics generalized Born surface area (MM/GBSA).<sup>30</sup> To calculate the ligand-binding free energies, a set of snapshots was selected from the 200-ns MD simulations of the WT and mutant system. More specifically, we focused on a time region from 25 ns to 50 ns of each trajectory. During this time region, each ligand maintained its binding with each pocket in all the trajectories. Therefore, we selected 25 snapshots from each 25-ns trajectory. Finally, we selected 125 snapshots (25 snapshots  $\times$  5 runs) to calculate each ligand-binding free energy for each complex based on MM/GBSA.

## 3. Results

### 3.1 Mutational Effects on the Ligand-Binding Pocket of T1r2aLBD

For the direct interaction with the ligand (L-Gln), the serine residues (Ser142 and Ser165) nearby the

ligand-binding pocket are conserved in amino acid sensing taste receptors T1r1 and most classes of C GPCRs.<sup>6</sup> Especially, Ser165 contacted with the L-Gln directly in the crystal structure. This tight interaction was commonly observed in other amino acids (Ala, Arg, Glu, and Gly), indicating that this direct interaction between the L-Gln and the binding pocket might play an essential role in taste recognition. Experimentally, mutagenesis of the human T1r (S165I and S165A for T1r2LBD) reportedly resulted in the loss of or a weakened response to L-amino acids.<sup>19</sup> Therefore, we regarded Ser165 as a key residue for investigation in medaka fish based on the mutational analyses of the human T1r. In this study, we reconsidered the direct interaction between the L-Gln and Ser165 of T1r2aLBD in medaka fish. To computationally address the mutational effect on Ser165, a set of MD simulations was performed on two types of mutants (Type #2 and #3 in Table 1). For Type #2 and Type #3, only T1r2aLBD of the WT heterodimer was mutated as follows: T1r2aLBD S165I – T1r3LBD WT and T1r2aLBD S165A – T1r3LBD WT, respectively.

To address the ligand-binding state of T1r2aLBD, the distance between the center of mass of L-Gln and the C<sub>α</sub> atom of the 165<sup>th</sup> residue was monitored. Figures 2(a-c) show a set of profiles of the distance versus simulation time for the WT and mutant system. As shown in Fig. 2(a), the ligand dissociated from the binding pocket in one of the five MD runs on the WT system. In contrast, as shown in Figs. 2(b-c), the distance rapidly increased in the profiles of these mutant systems. Quantitatively, the L-Gln completely dissociated in three (four) of the five MD runs on T1r2aLBD S165I (T1r2aLBD S165A). Therefore, these point mutations of Ser165 clearly changed the structural stability of the ligand-binding form, indicating that Ser165 of T1r2aLBD is a key residue to maintain its ligand-binding pocket.

To evaluate the ligand-binding ability of T1r2aLBD more quantitatively, the ligand-binding free

energies ( $\Delta G_{\text{bind}}$ ) were calculated for these systems using the `gmx_MMPBSA` tool<sup>31</sup> (Fig. 3(a)). To show the ligand-binding abilities of T1r2aLBD depending on the point mutations more clearly, we decomposed  $\Delta G_{\text{bind}}$  into the contributions from the mutated point (the 165<sup>th</sup> residue of T1r2aLBD) and calculated the interaction energies between the L-Gln and the mutated point ( $IE_{\text{ligand}}$ ) (Fig. 3(c)). Judging from these  $IE_{\text{ligand}}$  values, the S165A mutant system tends to bind to the L-Gln more weakly than the WT system owing to the lack of a hydrogen bond between the side chains of Ser165 and the L-Gln. Due to the lack of this interaction, the S165A mutant system tends to dissociate from the L-Gln more frequently than the others, supporting the ligand-dissociating profiles of T1r2aLBD (Fig. 2(c)). Compared to the S165A mutant system, the  $IE_{\text{ligand}}$  value of the S165I mutant system was comparable with that of the WT system (Fig. 3(c)). Therefore, the ligand-binding position of the S165I mutant system is similar to that of the WT system. As shown in Fig. 4(a), around the ligand-binding pocket, three hydrogen bonds were formed by the surrounding hydrophilic moieties with the C-terminal of L-Gln, resulting in an almost comparable ligand-binding interaction between the WT and S165I systems.

### 3.2 Mutational Effects on the Ligand-Binding Pocket of T1r3LBD

Figure 1(c) shows the arrangement of the key residues nearby the binding pocket of T1r3LBD in the X-ray crystal structure. As shown in Fig. 1(c), the  $\alpha$ -amino and carboxyl groups of L-Gln form hydrogen bonds with Ser150 and Thr173 nearby the binding pocket of T1r3LBD. Furthermore, the  $\alpha$ -amino group of L-Gln forms a water-mediated hydrogen bond with the side-chain hydroxyl group of Ser300 in LB2 of T1r3LBD (Fig. 1(c)). This single hydrogen bond might maintain the closed configuration of T1r3LBD by connecting

LB1 and LB2 since there are no other significant interactions between the L-Gln and LB2. This findings indicate that Ser300 might be a key residue for recognizing the L-Gln. In a previous study, to address how the ligand-binding response is affected by a mutation, the residue 300 of T1r3LBD human T1r was mutated from Ser to Glu.<sup>19</sup> This point mutation stabilized the ligand-binding form of T1r3LBD. In this study, based on this experimental evidence for the human T1r, Ser300 of T1r3LBD in medaka fish was mutated to Glu (Type #4 in Table 1) to computationally address the mutational effect nearby the ligand-binding pocket. For Type #4, only T1r3LBD of the WT heterodimer was mutated as follows: T1r2aLBD WT – T1r3LBD S300E.

Figures 2(d) and (e) show the time series of the distance between the L-Gln and the ligand-binding pocket of T1r3LBD on the WT and S300E mutant systems (T1r3LBD S300E), respectively. In these profiles, the distances for both systems converged well and the ligand-binding form was maintained in all the MD runs. Therefore, this point mutation did not perturb the ligand-binding form of T1r3LBD. To evaluate the ligand-binding ability of T1r3LBD more quantitatively, the  $\Delta G_{\text{bind}}$  values for both systems were calculated using the `gmx_MMPBSA` tool<sup>31</sup> (Fig. 3(b)). The  $\Delta G_{\text{bind}}$  values were decomposed into contributions from the mutated point (the 300<sup>th</sup> residue of T1r3LBD; Fig. 3(d)), corresponding to the  $IE_{\text{ligand}}$  values for both systems. Judging from the  $IE_{\text{ligand}}$  values, the S300E mutant system tends to bind to the ligand more strongly than the WT system. As a reason to maintain the binding form of this mutant, the water-mediated hydrogen bond between the L-Gln and Ser300 found in the WT system was replaced with a direct hydrogen bond between the  $\alpha$ -amino group of L-Gln and the side-chain carboxyl group of E300 (Fig. 4(c)). Therefore, LB1 and LB2 of T1r3LBD was connected by the newly formed direct hydrogen bond between the L-Gln and Glu300.

Next, another mutant system (T1r3LBD S300A) was created to weaken the hydrogen bond between

the L-Gln and Ser300 of T1r3LBD. In this study, Ser300 was simply mutated to a hydrophobic residue (Ala) (Type #5 in Table 1). For Type #5, only T1r3LBD of the WT heterodimer was mutated as follows: T1r2aLBD WT – T1r3LBD S300A. Figure 2(f) shows the time series of the distance between the L-Gln and the binding pocket of T1r3LBD. T1r3LBD maintained its ligand-binding form in all the MD runs, indicating that this point mutation did not affect the ligand-binding ability of T1r3LBD. As a quantitative evaluation of the ligand-binding ability of T1r3LBD, the  $\Delta G_{\text{bind}}$  values of the WT and S300A mutant systems were calculated (Fig. 3(b)). In addition, Figure 3(d) shows the  $IE_{\text{ligand}}$  values between the L-Gln and the mutated point (the 300<sup>th</sup> residue of T1r3LBD). Judging from the  $IE_{\text{ligand}}$  values, the S300A mutant system tends to bind to the L-Gln more strongly than the WT system, although the S300E mutant system showed the highest ligand-binding ability among all the systems. For the S300A mutant system, the L-Gln directly formed a hydrogen bond between its side-chain carbonyl group and the side-chain hydroxyl group of Ser301 instead of the water-mediated indirect interaction (Fig. 4(d)), which might be one of the reasons why the S300A mutant system bound strongly to the L-Gln. Interestingly, unlike T1r2LBD, T1r3LBD S300A increased the ligand-binding free energy, implying that Ser300 is not optimal for the recognition of the L-Gln. It is likely that Ser300 is more sensitive to the other taste ligands than the L-Gln. We will investigate the characteristics of other taste ligands and the role of Ser300 in the taste recognition elsewhere.

### 3.3 Different Structural Fluctuations of T1r2aLBD and T1r3LBD

To address how this heterodimer efficiently recognize taste substances dynamically, we evaluated structural fluctuations of both LBDs based on principal component analysis (PCA).<sup>32, 33</sup> Multiple trajectories

of the WT bound with the L-Gln from 25 ns to 50 ns (5 runs of 25 ns, 125 ns in total) was used to perform PCA. Figures 5(a-b) show the structural fluctuations of T1r2aLBD WT and T1r3LBD WT characterized by the 1<sup>st</sup> principle mode, respectively. As shown in Fig. 5(a), the 1<sup>st</sup> principal mode of T1r2aLBD WT characterized the hinge-bending motion between LB1 and Lb2 upon the ligand binding. Both LB1 and LB2 of T1r2aLBD WT fluctuated significantly compared to those of T1r3LBD WT. Therefore, T1r2aLBD WT flexibly changes the ligand-binding pocket using this hinge-bending motion. Owing to this characteristic domain motion, T1r2aLBD WT might promote associations/dissociations of each taste substance frequently. On the contrary, T1r3LBD WT did not show characteristic domain motions. Indeed, only LB2 of T1r3LBD WT fluctuated, while LB1 did not fluctuate significantly except for the loop regions. Judging from this non-characteristic domain motion, T1r3LBD WT might possess a rigid ligand-binding pocket to recognize each taste substance non-specifically without large domain motions.

#### 4. Discussion

Our mutational analyses based on the all-atom MD simulations provide useful information on the interaction changes of the L-Gln with other residues nearby each ligand-binding pocket in the atomic level. Therefore, we here discuss the interaction changes derived from our *in silico* mutations on T1r2aLBD and T1r3LBD in detail. For T1r2aLBD, the direct interactions with the L-Gln were significantly weakened in the S165I and S165A mutant systems. In both systems, the L-Gln tends to fluctuate owing to the loss of the hydrogen bond between the main-chain  $\alpha$ -amino group of L-Gln and the side-chain groups of Ile165 and Ala165 (Figs. 4(a-b)). Interestingly, only the S165A mutant caused

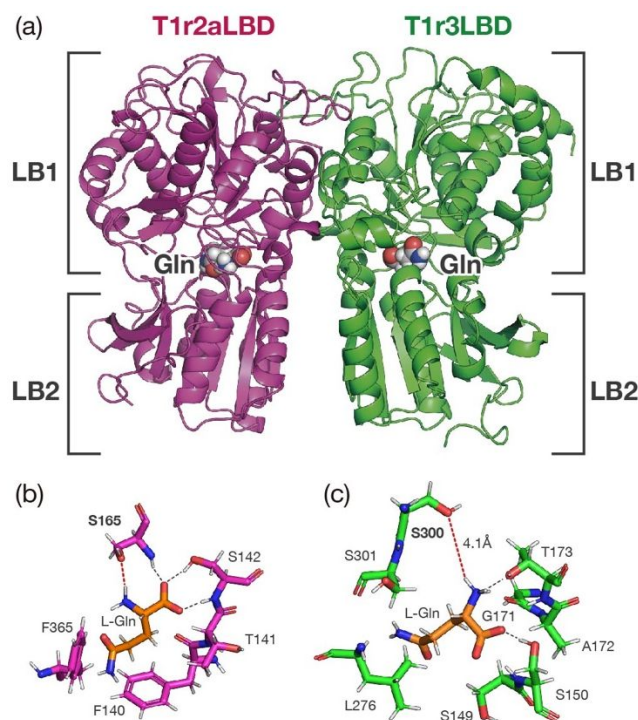
the loss of interaction between the side chain of Ser142 and the L-Gln (Fig. 4(b)), while the S165I mutant retained the same interaction found in the WT system (Fig. 4(a)). Therefore, the point mutations on S165 of T1r2aLBD changed the interactions with the key residue (Ser142) nearby its ligand-binding pocket. These mutational analyses provide evidence that the ligand-binding pocket of T1r2aLBD is sensitive to amino acid mutations. To maintain the ligand-binding form of T1r2aLBD, it is required that this pocket is composed of a set of specific residues. For T1r3LBD, the S300E and S300A mutant systems almost maintained their ligand-binding forms as found in the WT system. Indeed, the water-mediated indirect interaction found in the WT system was replaced with direct hydrogen bonds between the L-Gln and the alternative residues in both systems. Owing to the alternative hydrogen bonds with the L-Gln, both systems seemed to maintain their binding forms. In addition, both systems retained the interaction between the side chain of S150 and the L-Gln (Figs. 4(c-d)) after these point mutations. Therefore, these mutational analyses provide evidence that the ligand-binding pocket of T1r3LBD is robust to withstand amino acid mutations.

For T1r2aLBD and T1r3LBD, their different ligand-binding abilities might provide multiple binding modes that might be helpful for discriminating various taste substances efficiently. Furthermore, the dynamical analysis based on PCA indicates that T1r2aLBD possesses a flexible ligand-binding pocket, while T1r3LBD possesses a rigid ligand-binding pocket. Therefore, these different flexibilities in both ligand-binding pockets also provide multiple binding modes for discriminating taste substances efficiently.

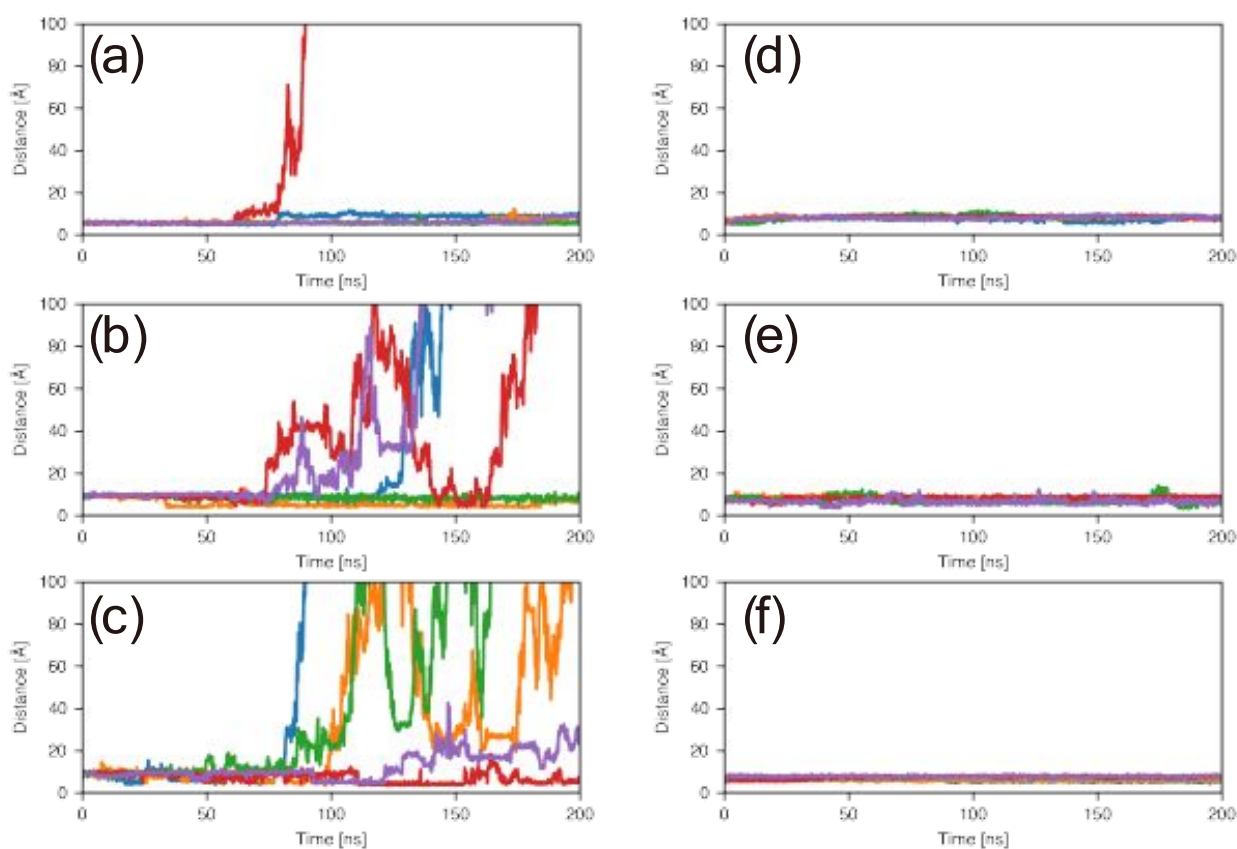
## 5. Conclusion

In this study, we performed a set of all-atom MD simulations on the extracellular LBDs of medaka fish T1r to computationally address the mutational effects on the key residues nearby each ligand-binding pocket in recognizing the ligand (L-Gln) using the WT and mutant systems. For T1r2aLBD, Ser165 in LB1 was important in ligand recognition owing to its direct hydrogen bond with the ligand. After mutating Ser165 to Ile or Ala, the direct hydrogen bonds between the ligand and the binding pocket were weakened, which destabilized the ligand-binding form of T1r2aLBD. For T1r3LBD, Ser300 in LB2 was important in the ligand recognition since the water-mediated hydrogen bond with the side-chain hydroxyl group of Ser300 in LB2 of T1r3LBD is a single interaction that connects LB1 and LB2. After mutating Ser300 to Glu or Ala, both mutant system almost maintained their ligand-binding form of T1r3LBD. As a mechanism for maintaining the binding form of T1r3LBD, alternative hydrogen bonds were formed as direct interactions instead of the indirect water-mediated interactions found in the WT system, which stabilized the binding form of T1r3LBD by connecting LB1 and LB2. These different ligand-binding abilities of both LBDs derived from our mutational analyses were quantitatively confirmed by calculating their ligand-binding free energies based on MM/GBSA.

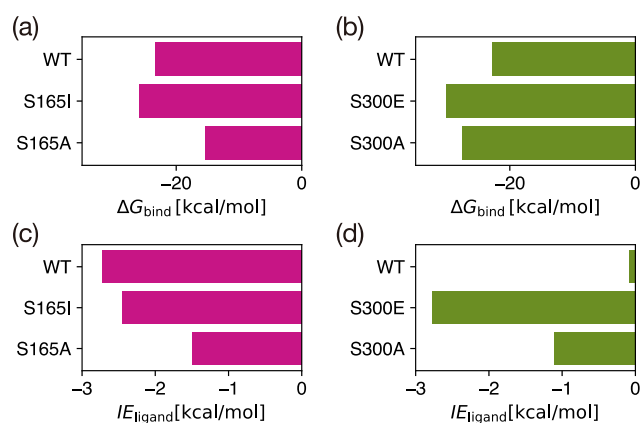
Judging from our *in silico* mutational analyses, T1r2aLBD was structurally destabilized by the amino acid mutations. Therefore, it might be required that the ligand-binding pocket of T1r2aLBD is composed of a set of specific residues to maintain its ligand-binding form. In contrast, T1r3LBD was robust to withstand the amino acid mutations. Therefore, these different ligand-binding abilities of both LBDs provide multiple binding modes, which might be helpful for discriminating various taste substances or detecting concentrations of nutrients efficiently.

**Figure 1**

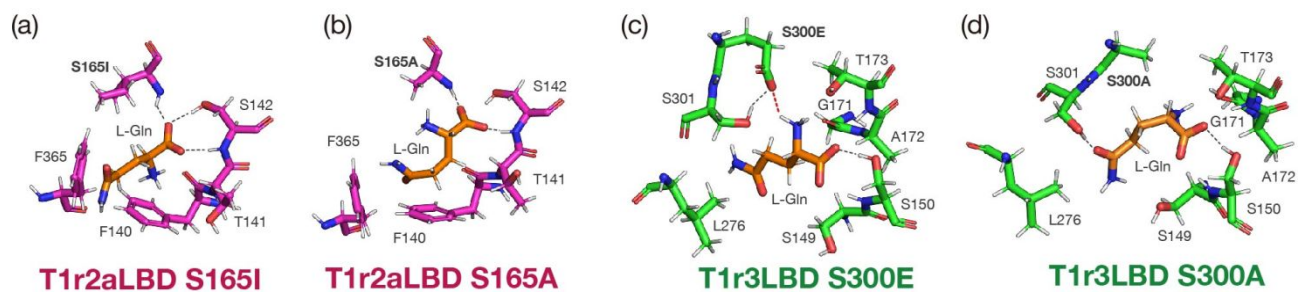
X-ray crystal structure of taste receptor. (a) Heterodimer (extracellular LBDs of the medaka fish T1r) composing of T1r2aLBD (purple) and T1r3LBD (green) with the ligand (L-Gln). The L-Gln is drawn with a van der Waals (VDW) representation. For T1r2aLBD and T1r3LBD, their ligand-binding domains (LB1 and LB2) are specified. The key residues nearby each ligand-binding pocket of (b) T1r2aLBD and (c) T1r3LBD. The representative hydrogen bonds are highlighted with dashed lines.

**Figure 2**

Time series of the distance between the ligand and each ligand-binding pocket. (a) T1r2aLBD WT, (b) T1r2aLBD S165I, (c) T1r2aLBD S165A, (d) T1r3LBD WT, (e) T1r3LBD S300E, and (f) T1r3LBD S300A. The line colors represent five MD runs performed by changing their initial velocities independently.

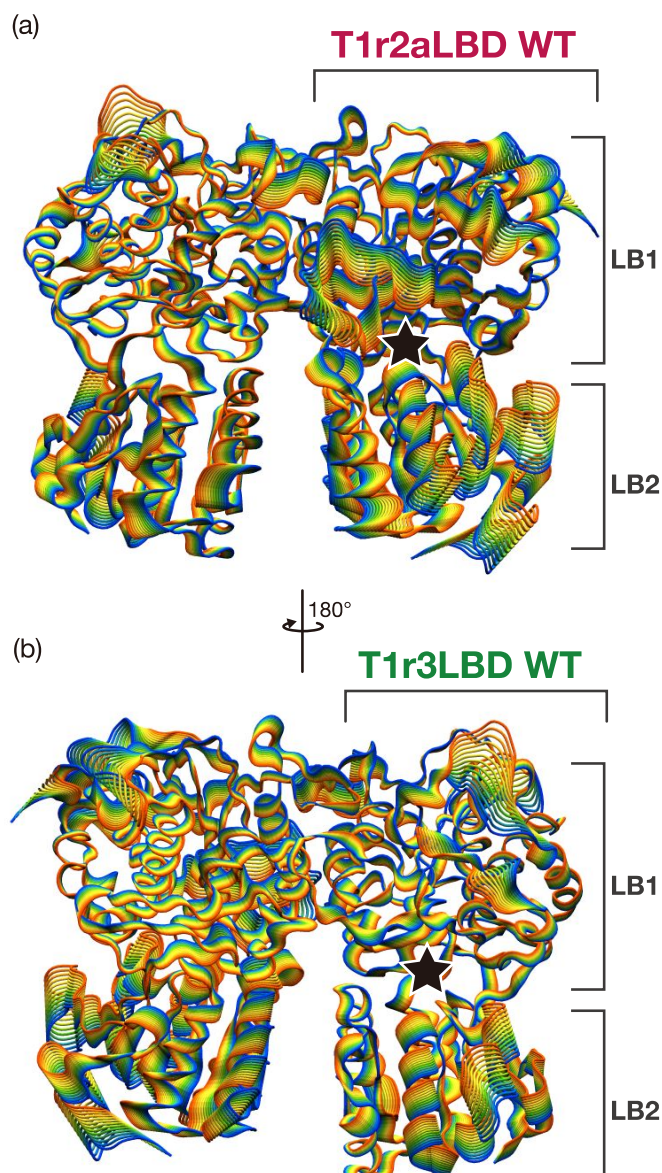
**Figure 3**

Ligand-binding free energies and their decompositions into interactions energies between the ligand and each mutated point. The upper panels display the ligand-binding free energies ( $\Delta G_{\text{bind}}$ ) of (a) T1r2aLBD and (b) T1r3LBD. The lower panels display the interaction energies between the ligand and each mutated point ( $I E_{\text{ligand}}$ ) of (c) T1r2aLBD and (d) T1r3LBD. The averages and standard deviations of the energies are presented in Table 2.

**Figure 4**

The key residues nearby each ligand-binding pocket. (a) T1r2aLBD S165I, (b) T1r2aLBD S165A, (c) T1r3LBD S300E, and (d) T1r3LBD S300A. The representative hydrogen bonds are depicted with dashed lines.

Figure 5



Structural fluctuations of (a) T1r2aLBD WT and (b) T1r3LBD WT bound with the ligands characterized by the 1<sup>st</sup> principal mode. The positions of the ligands are marked with stars. The color gradation represents the magnitudes of the structural fluctuations (yellow: averages, red/blue: structures that highly deviate from the averages).

**Table 1**

MD conditions of five types of heterodimers (the WT and mutant systems of the extracellular LBDs of the medaka fish T1r) depending on the mutational states of both LBDs (T1r2aLBD and T1r3LBD). Type #1 represents the WT heterodimer without mutations. The others (Type #2, #3, #4, and #5) represent mutant systems. In this study, one of the monomers (T1r2aLBD or T1r3LBD) was mutated.

<b>Type of heterodimer</b>	<b>T1r2aLBD</b>	<b>T1r3LBD</b>	<b>Simulation time [ns]</b>	<b>Number of MD runs</b>
#1	WT	WT	200	5
#2	S165I	WT	200	5
#3	S165A	WT	200	5
#4	WT	S300E	200	5
#5	WT	S300A	200	5

**Table 2**

$\Delta G_{\text{bind}}$ : Ligand-binding free energy of each monomer (T1r2aLBD or T1r3LBD). To calculate  $\Delta G_{\text{bind}}$  based on MM/GBSA, we used 125 (25 snapshots  $\times$  5 runs) snapshots for each complex, where these 25 snapshots were distributed in each trajectory from 25 ns to 50 ns.

Type of Heterodimer	$\Delta G_{\text{bind}}$ (T1r2aLBD) [kcal/mol]	$\Delta G_{\text{bind}}$ (T1r3LBD) [kcal/mol]	$IE_{\text{ligand}}$ (T1r2aLBD) [kcal/mol]	$IE_{\text{ligand}}$ (T1r3LBD) [kcal/mol]
#1	$-23.3 \pm 4.2$	$-22.8 \pm 4.7$	$-2.7 \pm 1.4$	$-0.1 \pm 0.3$
#2	$-25.9 \pm 7.3$	—	$-2.5 \pm 0.8$	—
#3	$-15.4 \pm 6.4$	—	$-1.5 \pm 1.0$	—
#4	—	$-30.1 \pm 10.1$	—	$-2.8 \pm 2.7$
#5	—	$-27.6 \pm 5.0$	—	$-1.1 \pm 1.6$

$IE_{\text{ligand}}$ : Interaction energy between the ligand (L-Gln) and each mutated point (the 165<sup>th</sup> residue of T1r2aLBD or the 300<sup>th</sup> residue of T1r3LBD)

## Acknowledgement

This research was partially supported by the Initiative on Promotion of Supercomputing for Young or Women Researchers, Information Technology Center, University of Tokyo. YS acknowledges support from the CREST program (grant No. JPMJCR20B3) by the Japan Agency for Science and Technology (JST) and Grant-in-aid for innovative research “Biometal Sciences” (grant No. 20H05497) by the Ministry of Education, Culture, Sports, Science and Technology (MEXT), Japan. RH acknowledges support from Japan Society for the Promotion of Science (JSPS) KAKENHI under Grant Numbers JP21K06094.

## References

1. J. Chandrashekar, M. A. Hoon, N. J. P. Ryba and C. S. Zuker, *Nature*, 2006, **444**, 288-294.
2. D. A. Yarmolinsky, C. S. Zuker and N. J. P. Ryba, *Cell*, 2009, **139**, 234-244.
3. G. Nelson, M. A. Hoon, J. Chandrashekar, Y. F. Zhang, N. J. P. Ryba and C. S. Zuker, *Cell*, 2001, **106**, 381-390.
4. X. D. Li, L. Staszewski, H. Xu, K. Durick, M. Zoller and E. Adler, *Proc. Natl. Acad. Sci. U. S. A.*, 2002, **99**, 4692-4696.
5. G. Nelson, J. Chandrashekar, M. A. Hoon, L. X. Feng, G. Zhao, N. J. P. Ryba and C. S. Zuker, *Nature*, 2002, **416**, 199-202.
6. J. P. Pin, T. Galvez and L. Prezeau, *Pharmacol. Ther.*, 2003, **98**, 325-354.
7. P. Shi and J. Z. Zhang, *Mol. Biol. Evol.*, 2006, **23**, 292-300.
8. M. W. Baldwin, Y. Toda, T. Nakagita, M. J. O'Connell, K. C. Klasing, T. Misaka, S. V. Edwards and S. D. Liberles, *Science*, 2014, **345**, 929-933.
9. H. Xu, L. Staszewski, H. X. Tang, E. Adler, M. Zoller and X. D. Li, *Proc. Natl. Acad. Sci. U. S. A.*, 2004, **101**, 14258-14263.
10. G. Morini, A. Bassoli and P. A. Temussi, *J. Med. Chem.*, 2005, **48**, 5520-5529.
11. F. Zhang, B. Klebansky, R. M. Fine, H. Xu, A. Pronin, H. T. Liu, C. Tachdjian and X. D. Li, *Proc. Natl. Acad. Sci. U. S. A.*, 2008, **105**, 20930-20934.
12. J. J. L. Cascales, S. D. O. Costa, B. L. de Groot and D. E. Walters, *Biophys. Chem.*, 2010, **152**, 139-144.
13. K. Masuda, A. Koizumi, K. Nakajima, T. Tanaka, K. Abe, T. Misaka and M. Ishiguro, *PLoS One*, 2012, **7**.
14. Y. Toda, T. Nakagita, T. Hayakawa, S. Okada, M. Narukawa, H. Imai, Y. Ishimaru and T. Misaka, *J. Biol. Chem.*, 2013, **288**, 36863-36877.
15. E. L. Maillet, M. Cui, P. H. Jiang, M. Mezei, E. Hecht, J. Quijada, R. F. Margolskee, R. Osman and

- M. Max, *Chem. Senses*, 2015, **40**, 577-586.
16. N. Kunishima, Y. Shimada, Y. Tsuji, T. Sato, M. Yamamoto, T. Kumasaka, S. Nakanishi, H. Jingami and K. Morikawa, *Nature*, 2000, **407**, 971-977.
  17. Y. Geng, M. Bush, L. Mosyak, F. Wang and Q. R. Fan, *Nature*, 2013, **504**, 254-259.
  18. E. Nango, S. Akiyama, S. Maki-Yonekura, Y. Ashikawa, Y. Kusakabe, E. Krayukhina, T. Maruno, S. Uchiyama, N. Nuemket, K. Yonekura, M. Shimizu, N. Atsumi, N. Yasui, T. Hikima, M. Yamamoto, Y. Kobayashi and A. Yamashita, *Sci. Rep.*, 2016, **6**, 25745-25741-25748.
  19. N. Nuemket, N. Yasui, Y. Kusakabe, Y. Nomura, N. Atsumi, S. Akiyama, E. Nango, Y. Kato, M. K. Kaneko, J. Takagi, M. Hosotani and A. Yamashita, *Nat Commun*, 2017, **8**, 15530-15531-15510.
  20. W. L. Jorgensen, J. Chandrasekhar, J. D. Madura, R. W. Impey and M. L. Klein, *J. Chem. Phys.*, 1983, **79**, 926-935.
  21. M. J. Abraham, D. van der Spoel, E. Lindahl and B. Hess, The GROMACS Development Team, GROMACS User Manual 2019, [www.gromacs.org](http://www.gromacs.org).
  22. B. Hess, H. Bekker, H. J. C. Berendsen and J. G. E. M. Fraaije, *J. Comput. Chem.*, 1997, **18**, 1463-1472.
  23. S. Miyamoto and P. A. Kollman, *J. Comput. Chem.*, 1992, **13**, 952-962.
  24. G. Bussi, D. Donadio and M. Parrinello, *J. Chem. Phys.*, 2007, **126**, 014101-1-7.
  25. M. Parrinello and A. Rahman, *Phys. Rev. Lett.*, 1980, **45**, 1196-1199.
  26. M. Parrinello and A. Rahman, *J. Appl. Phys.*, 1981, **52**, 7182-7190.
  27. U. Essmann, L. Perera, M. L. Berkowitz, T. Darden, H. Lee and L. G. Pedersen, *J. Chem. Phys.*, 1995, **103**, 8577-8593.
  28. Y. Duan, C. Wu, S. Chowdhury, M. C. Lee, G. M. Xiong, W. Zhang, R. Yang, P. Cieplak, R. Luo, T. Lee, J. Caldwell, J. M. Wang and P. Kollman, *J. Comput. Chem.*, 2003, **24**, 1999-2012.
  29. D.A. Case, H.M. Aktulga, K. Belfon, I.Y. Ben-Shalom, S.R. Brozell, D.S. Cerutti, T.E. Cheatham, III, V.W.D. Cruzeiro, T.A. Darden, R.E. Duke, G. Giambasu, M.K. Gilson, H. Gohlke, A.W. Goetz, R. Harris, S. Izadi, S.A. Izmailov, C. Jin, K. Kasavajhala, M.C. Kaymak, E. King, A. Kovalenko, T. Kurtzman, T.S. Lee, S. LeGrand, P. Li, C. Lin, J. Liu, T. Luchko, R. Luo, M. Machado, V. Man, M. Manathunga, K.M. Merz, Y. Miao, O. Mikhailovskii, G. Monard, H. Nguyen, K.A. O'Hearn, A. Onufriev, F. Pan, S. Pantano, R. Qi, A. Rahnamoun, D.R. Roe, A. Roitberg, C. Sagui, S. Schott-Verdugo, J. Shen, C.L. Simmerling, N.R. Skrynnikov, J. Smith, J. Swails, R.C. Walker, J. Wang, H. Wei, R.M. Wolf, X. Wu, Y. Xue, D.M. York, S. Zhao, and P.A. Kollman (2021), Amber 2021, University of California, San Francisco.
  30. B. R. Miller, T. D. McGee, J. M. Swails, N. Homeyer, H. Gohlke and A. E. Roitberg, *J. Chem. Theory Comput.*, 2012, **8**, 3314-3321.
  31. M. E. V.-T. Mario S. Valdés Tresanco, Pedro A. Valiente, & Ernesto Moreno Frías, **DOI: <http://doi.org/10.5281/zenodo.4569307>**.
  32. A. Kitao, F. Hirata and N. Go, *Chem. Phys.*, 1991, **158**, 447-472.
  33. A. Amadei, A. B. M. Linssen and H. J. C. Berendsen, *Proteins-Structure Function and Genetics*, 1993, **17**, 412-425.